Role of Anions in Aqueous Sol−Gel Process Enabling Flexible Cu(In,Ga)S₂ Thin-Film Solar Cells

Yunjung Oh,[†] Kyoohee Woo,[‡] Daehee Lee,[†] Hongseuk Lee,[†] Kyujin Kim,[†] Inhyuk Kim,[†] Zhaoyang Zhong,[†] Sunho Jeong,[§] and Jooho Moon*,[†]

[†]Department of Materials Science and Engineering, Yonsei University, 50 Yonsei-ro Seodaemun-gu, Seoul 120-749, Republic of Korea

[‡]Advanced Manufacturing Systems Research Division, Korea Institute of Machinery and Materials, 156 Gajeongbuk-ro, Yuseong-gu, Daejeon 305-343, Republic of Korea

[§]Division of Advanced Materials, Korea Research Institute of Chemical Technology, 19 Sinseongno, Yuseong-gu, Daejeon 305-600, Republic of Korea

Ⓢ *Supporting Information*

ABSTRACT: Recently, environmental-friendly, solution-processed, flexible Cu-(In,Ga)(S,Se)₂ devices have gained significant interest, primarily because the solution deposition method enables large-scale and low-cost production of photovoltaics, and a flexible substrate can be implemented on uneven surfaces in various applications. Here, we suggest a novel green-chemistry aqueous ink that is readily achievable through the incorporation of molecular precursors in an aqueous medium. A copper formate precursor was introduced to lower the fabrication temperature, provide compatibility with a polyimide plastic substrate, and allow for high photovoltaic performance. Through a comparative spectroscopic study on temperature-dependent chemical/ crystal structural evolution, the chemical role of copper formate was elucidated, which led to the chalcopyrite framework that was appropriate to low-temperature annealed Cu(In,Ga)S₂ absorber layers at 400 °C. This Cu(In,Ga)S₂ solar cell exhibited a power conversion efficiency of 7.04% on a rigid substrate and 5.60% on a polymeric substrate. Our cell on the polymeric substrate also demonstrated both acceptable mechanical flexibility and durability throughout a repeated bending test of 200 cycles.

KEYWORDS: *flexible thin-film solar cells, CIGS, aqueous sol−gel, low temperature processing*
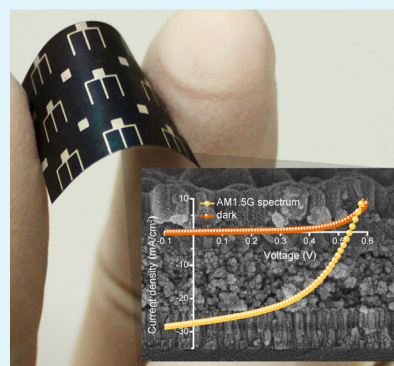
1. INTRODUCTION

Cu(In,Ga)(S,Se)₂ (CIGS) is a promising absorber material that can be utilized in highly efficient photovoltaic devices, owing to its characteristic optoelectronic properties. In particular, solution-processed CIGS solar cells have gained tremendous interest, as solution deposition methods allow for scalable, low-cost production.[1,2] Todorov et al. demonstrated that solution process-based devices can achieve high performance, along with economical synthetic production. In these studies, an efficiency as high as 15.2% was reported for CIGS thin-film solar cells, which were fabricated by solution process using hydrazine as a solvent.[3] However, due to the highly toxic and explosive chemical nature of hydrazine solvent, this commonly employed strategy has drawbacks in terms of processing when considering the scalability for practical applications. Recently, there has been a move to utilize solution processes employing a environmentally benign, nonflammable solvent for generating high performance CIGS solar cells. Among the various chemical approaches, it has been recently demonstrated that the nontoxic solvent-based sol−gel route can be successfully employed in producing device-quality CIGS absorber layers with a power conversion efficiency (PCE) of 7.7−8.3%.[4,5] In addition to the necessity of green chemistry-based method-

ology, the realization of low-temperature processes to generate flexible CIGS devices is currently being actively researched.

To date, sol−gel chemistry has been employed with alcohol as a solvent medium; this conventional chemical pathway yielded the possibility for 7−8% efficient CIGS devices on a rigid glass substrate after annealing at temperatures above 500 °C.[4] Even with much effort using various precursors and additive-based functional ink formulations, polymeric substrate-based flexible solution-processed CIGS solar cells have not yet been demonstrated. CIGS solar cells on flexible substrates offer several advantages over their rigid, glass substrate-based counterparts.[6,7] They can be used on uneven surfaces even for wearable and rugged, rollable applications and can have a lower the manufacturing cost when applied to continuous roll-to-roll fabrication. The most widely used flexible substrates include metal foils and plastics such as polyimide (PI). Especially, PI is free of metallic impurities and is also capable of inhibiting the formation of an insulating layer. However, PI is more temperature-sensitive than metal foils and only allows for

a limited processing temperature below 450 °C. Therefore, in order to fully realize the advantages of flexible solar cells in terms of low-cost and scalability, the low-temperature solution processing, compatible with temperature-sensitive flexible substrates, is highly desirable.[8]

In addition, compared with conventional alcohol-based sol−gel chemistry, aqueous-based pathways have various advantages. Metal cations, derived from metal salt precursors in a specific solvent medium, undergo subsequent chemical reactions of water molecule solvation, hydrolysis, and condensation, leading to an oxide framework skeleton, which is in turn converted into desirable selenide/sulfide compounds under a S/Se atmosphere at elevated temperatures. The degree of oxide framework formation, which is generated by consuming hydroxide and the precursor compound itself, is highly dependent on the chemical reaction of water molecules. The incorporation of a proper amount of water molecules is critical to tailor accurately the sol−gel chemical reaction under specific atmospheric conditions. Therefore, the sol−gel reaction is inevitably sensitive to the environmental conditions. However, the aqueous solvent system already has provided excessive water molecules to sol−gel reaction, so this system is insensitive to humidity in an ambient environment.[9] Most importantly, the aqueous solvent is more environmentally friendly compared to alcohol-based solvents, which provides the basic potential for practical applications requiring strict safety prerequisites in mass production.

Here, we demonstrate solution-processed flexible $Cu(In,Ga)S_2$ solar cells fabricated on a PI substrate at a low temperature (≤ 400 °C), using a simple, nontoxic, green chemistry aqueous ink. To facilitate a low-temperature processable, high-performance aqueous ink, a stable Cu−In−Ga aqueous precursor solution is introduced, without the addition of any stabilizer or binder, by employing a heretofore unexplored precursor, metal formate. The role of formate anion ($HCOO^-$) was clarified through a comparative analysis against conventional anions (Cl^- and NO_3^{3-}), in conjunction with an in-depth study on the temperature-dependent chemical/crystalline structural evolution in $Cu(In,Ga)S_2$ absorber films. Our aqueous precursor-derived $Cu(In,Ga)S_2$-based solar cells annealed at 400 °C exhibit a PCE of 7.04% on a rigid substrate and 5.60% on a PI flexible substrate. The purpose of this work is to demonstrate the possibility of fabricating CIGS solar cells at low temperatures, compatible with temperature-sensitive flexible substrates, using aqueous ink chemistry.

2. RESULTS AND DISCUSSION

We synthesized an aqueous ink by incorporating formate, which, to date, has not been studied in formulating functional inks for CIGS absorber layers. In conventional sol−gel-based CIGS ink formulations, the common precursors are nitrates and chlorides. In order to elucidate the influence of the anions on chemical evolutions in an aqueous system, three types of clear aqueous inks were prepared using either Cu formate (Cu-$(HCOO)_2$), Cu chloride ($CuCl_2$), or Cu nitrate ($Cu(NO_3)_2$). Meanwhile, In nitrate ($In(NO_3)_3$) and Ga nitrate ($Ga(NO_3)_3$) were used as the In/Ga cation source. To resolve the solubility problem, we dissolved either $Cu(HCOO)_2$, $CuCl_2$, or Cu-$(NO_3)_2$ together with $In(NO_3)_3$ and $Ga(NO_3)_3$. It should be noted that these salts are dissociated in water, so that the combination type of the dissociated anions can determine the pH of the aqueous solutions. The resulting aqueous precursor inks were multispin-coated onto a Mo-coated glass substrate,

followed by annealing at 350 °C in air to oxidize the films. Then, in order to convert into $Cu(In,Ga)S_2$ absorber layers, the preannealed films were further heat-treated under two consecutive atmospheres in a single annealing process: reduction during a ramping step in a gas mixture of H_2 (5%) and N_2, followed by sulfurization at a given target temperature in H_2S (5%) and N_2. We denote the films derived from the formate-containing ink, the chloride-containing ink, and all nitrate-based ink as F-CIGS, C-CIGS, and N-CIGS, respectively. The number followed by letters indicates the reduction/sulfurization temperature.

Thermo-gravimetry analysis (TGA) revealed the different decomposition behavior of precursor inks during annealing in air, as shown in Figure 1. The formate-containing ink (F-CIGS)
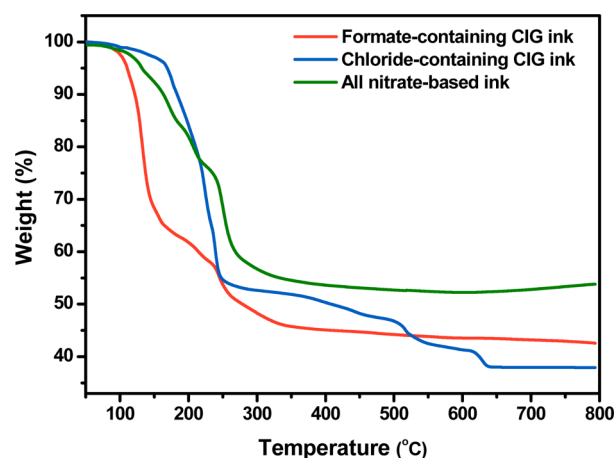
Figure 1. TG analysis of the aqueous-based Cu formate and In/Ga nitrate precursor ink. This analysis was performed in an air atmosphere (150 cc min^{-1}). Inks using Cu chloride or Cu nitrate instead of formate were also analyzed under the same conditions.

showed the significant weight loss around 350 °C without the further weight loss. On the other hand, the chloride-containing ink showed continuous weight loss until 650 °C, indicating that C-CIGS film annealed at 400 °C in air likely still contains decomposable impurities, which might prevent phase transformation and grain growth during sulfurization. We also prepared an ink using Cu nitrate and In/Ga nitrate to comparatively monitor the decomposition characteristics. All nitrate-based precursor ink (N-CIGS) exhibited similar decomposition behavior as the formate-containing ink revealed.

X-ray photoelectron spectroscopy (XPS)-based chemical analysis was performed to understand the influence of anion type on chemical phase evolution of $Cu(In,Ga)S_2$ films during the sequential annealing steps of air annealing, reduction, and sulfurization (Figure 2). The F-CIGS preannealed at 350 °C in air contained only the Cu(II)−O state at 933.5 eV, whereas the C-CIGS preannealed in air consisted of a mixed phase of Cu(II)−OH, Cu(II)−O, and Cu(II)−Cl.[10−12] The air-annealed N-CIGS also had the mixed state of Cu(II)−O and Cu(II)−OH. Different chemical states of indium were also detected depending on the anion type. Indium oxide was only present in a formate-based film, whereas indium hydroxide existed in a chloride-based film and a mixed state of hydroxide/oxide was observed in a nitrate based film (Figure S1 in Supporting Information). As to the chemical state of Ga, Ga−O state was observed in all three films. After reduction at 350 °C (Figure 2), the copper in F-CIGS showed a single bonding
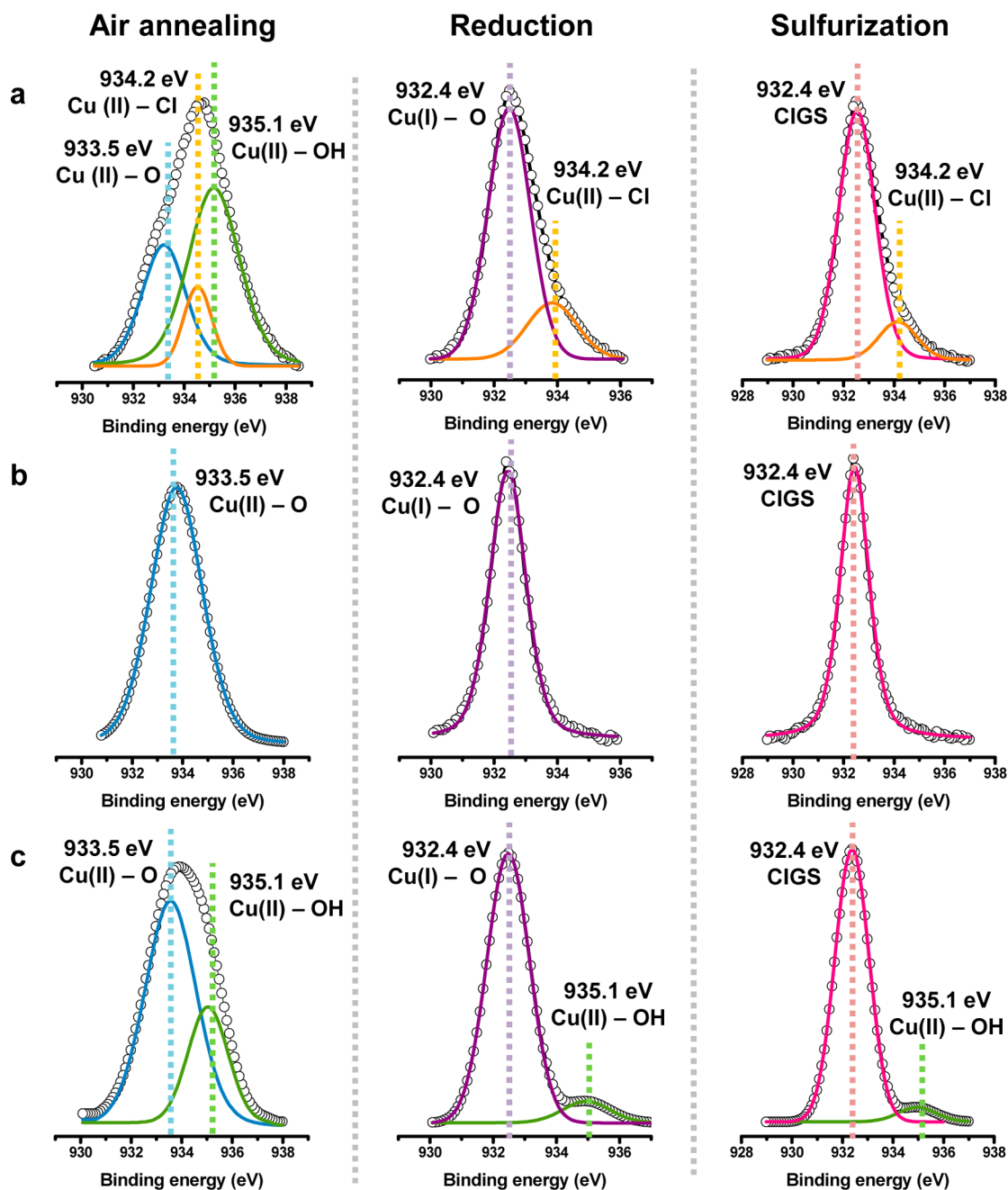
Figure 2. X-ray photoemission spectra of Cu $2p_{3/2}$ of the films using (a) chloride-containing ink, (b) formate-containing ink, and (c) all nitrate based ink during the sequential annealing steps of air annealing, reduction, and sulfurization at 350 °C.

state, which is assumed to be Cu(I)−O, indicating the incomplete reduction of the oxidized precursor film under H_2. After sulfurization at 350 °C, the F-CIGS revealed a Cu⁺ chemical bonding state in Cu(In,Ga)S₂, at 932.4 eV. This observation suggests the formation of CIGS as follows: (Cu−In−Ga Oxide) + H_2S → $Cu(In,Ga)S_2$ + H_2 + H_2O. On the other hand, even after reduction/sulfurization, a Cl impurity (Cu(II)−Cl) remained at 934.2 eV for C-CIGS and the N-CIGS film had hydroxyl group at 935.1 eV. For chemical states of In and Ga, there was no apparent difference between F-CIGS and C-CIGS after the reduction/sulfurization process (Figure S2 in Supporting Information).

These different chemical states among the annealed films are originated from the tendency of hydrolysis and condensation. In aqueous sol−gel system, hydrolysis and condensation

reaction rates is predominantly dependent on the pH of the system, i.e., hydroxo or oxo ligands are formed according to pH of the solution.[9] When the same metal cations are involved, the type of the anions plays a critical role in determining the pH and in turn the reaction pathways in aqueous sol−gel chemistries. Different anions dissociated from metal precursors behave differently in water solvents due to their distinctive natures. Formate anions (HCOO⁻) possess a higher basicity than chloride (Cl⁻) and nitrate (NO₃⁻) anions, and so generate OH⁻ anions more readily in an aqueous medium. These characteristics result in the different pH of the aqueous ink solutions; the formate-containing ink revealed the pH value of 1.8, while pH of chloride-containing and all nitrate-based inks were 0.3 and 0.8, respectively. A degree of hydrolysis and condensation reactions can be controlled by pH as described:[13]

$$[M - (OH_2)]^{z+} \leftrightarrow [M - OH]^{(z-1)+} + H^+$$
$$\leftrightarrow [M = O]^{(z-2)} + 2H^+$$
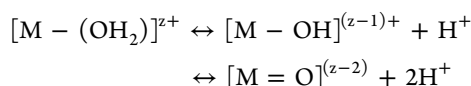
Acidic conditions hinder the deprotonation, resulting in the formation of hydroxo ligands, whereas oxo ligands can be formed easily in the presence of OH^-. In this regard, higher pH condition associated with formate-containing ink facilltates the formation of oxo ligands, leading to the M-O-M oxide framework through the oxidative annealing. XPS full scan analysis allowed us to calculate a relative ratio of oxygen to all metals for three CIGS samples preannealed at 350 °C in air, that is, 3.2 for F-CIGS, 3.54 for C-CIGS, and 3.78 for N-CIGS. This observation also supports that the formate-containing ink enables the formation of M−O−M framework as expressed by smaller oxygen-to-metal ratio. Nucleophilic strength, another chemical factor, was also involved in metal cation−anion pairs that were present in a solvent-free film layer after a coating/drying process. The stability of cation−anion pairs was predominantly determined by the anion's nucleophilic strength; the strength of Cl^- was greater than that of $HCOO^-$ (i.e., $Cl^- > NO^{3-} > HCOO^-$), which implies that a larger supply of thermal/chemical energy was required to decompose anions for generating an impurity-free CIGS absorber layer.[14,15] In addition, when taking into consideration the thermodynamic spontaneity of −O, −OH, and −Cl for the reaction with $H_2(g)$,[16] chlorine impurities in C-CIGS were not easily removed, even in a reactive hydrogen atmosphere at elevated temperatures. Thus, it is believed that the chemical nature of $HCOO^-$ allows the achievement of a pure, higher-quality oxide film at a temperature as low as 350 °C, and the oxide film is converted into a desirable $Cu(In,Ga)S_2$ phase by a low-temperature sulfurization process. We selected two extreme cases, formate-containing ink and chloride-containing ink, in order to further investigate the influence of anion type.

Figure 3a showed X-ray diffraction (XRD) results for the F-CIGS/C-CIGS films as a function of sulfurization temperature. In the case of films annealed at 350 °C, both films exhibited a peak at 2θ of 54−57°, which slightly shifted toward a lower angle with a broader shoulder (as shown in the enlarged Figure 3a), which is possibly due to the coexistence of secondary phases and a nonstoichiometric/nonchalcopyrite phase. By contrast, both samples annealed at 400 °C exhibited sharp peaks at 28.2, 46.75, and 55.5°, which are attributed to the diffraction of (112), (204/220), and (116/312) planes of the chalcopyrite structure (JCPDS no. 27-0159), respectively. This suggests that $Cu(In,Ga)S_2$ crystalline phase forms by the sequential reduction/sulfurization process even at 400 °C, regardless of the anion type. However, it should be noted that XRD alone is insufficient to accurately determine the phase purity of $Cu(In,Ga)S_2$ crystalline structure because many binary and ternary chalcogenides have similar crystal structures. Raman spectroscopy was utilized to obtain further insight into the phase identification (Figure 3b). The C-CIGS film was composed of undesirable Cu−Au ordered phases as well as chalcopyrite phase, even when annealed at 400 °C.[17−19] Also, C-CIGS films contains the peaks at 275 and 330 cm^{-1}, which indicated the presence of impurity phases such as a ternary sulfide ($CuIII_5S_8$), where III stands for In or Ga with a +3 oxidation state. By contrast, the F-CIGS400 film showed a sharp peak at 295 cm^{-1}, assigned as A_1 mode of chalcopyrite CIGS phase, although the F-CIGS350 film contained an Cu−Au ordered phase, as indicated by the peak at 309 cm^{-1}. This
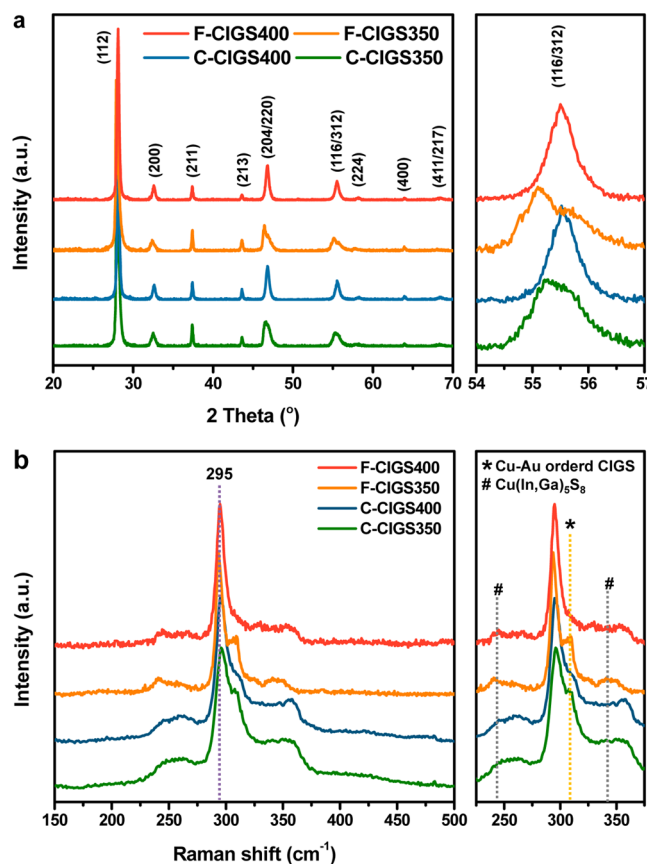
Figure 3. (a) XRD results of the CIGS film fabricated on glass using either formate-containing ink or chloride-containing ink as a function of the annealing temperature. Enlarged graphs in the 2θ angle range 54−57° are also displayed. (b) Raman spectra of the CIGS films as a function of sulfurization temperature. Enlarged graphs in the range from 225 to 375 cm^{-1} are also displayed. The CIGS films were annealed in a N_2 + H_2S (5%) atmosphere in a tubular furnace.

peak is clearly different from A_1 mode at 290 cm^{-1} of Ga-free $CuInS_2$, implying a peak shift due to the addition of Ga. It is believed that broad noise-like peaks in the range 230−360 cm^{-1} refer to B/E modes of chalcopyrite $Cu(In,Ga)S_2$.[20] However, it should be noted that the peak of ternary sulfide is located in the range of broad B/E mode peaks, suggesting a trace of ternary sulfide.

Figure 4a contains SEM images showing the microstructural evolution of absorber layers. For both inks, as the sulfurization temperature increased, the films were gradually densified with a coarsened grain feature. However, whereas C-CIGS films had a rough surface morphology, F-CIGS films showed a morphologically uniform surface structure. As mentioned above, the C-CIGS films annealed even at 350 °C in air still contained decomposable impurities, which might react with H_2S or H_2 gas during the sulfurization process. Therefore, it is speculated that the evolution of byproducts during the sulfurization induces a rough morphological surface with large voids. The surface composition of the F-CIGS400 film was determined by energy-dispersive X-ray spectroscopy (EDX), as listed in Table 1. It was clearly observed that the average composition of the sulfurized film was closer to the initial precursor composition. Figure S3 (Supporting Information) provides the cross-sectional microstructure image for the F-CIGS400-derived solar cell. The absorber film with a thickness of ∼1.0 μm consisted of a fine-grained sublayer and a large-grained outer

17743

dx.doi.org/10.1021/am504194t | ACS Appl. Mater. Interfaces 2014, 6, 17740−17747
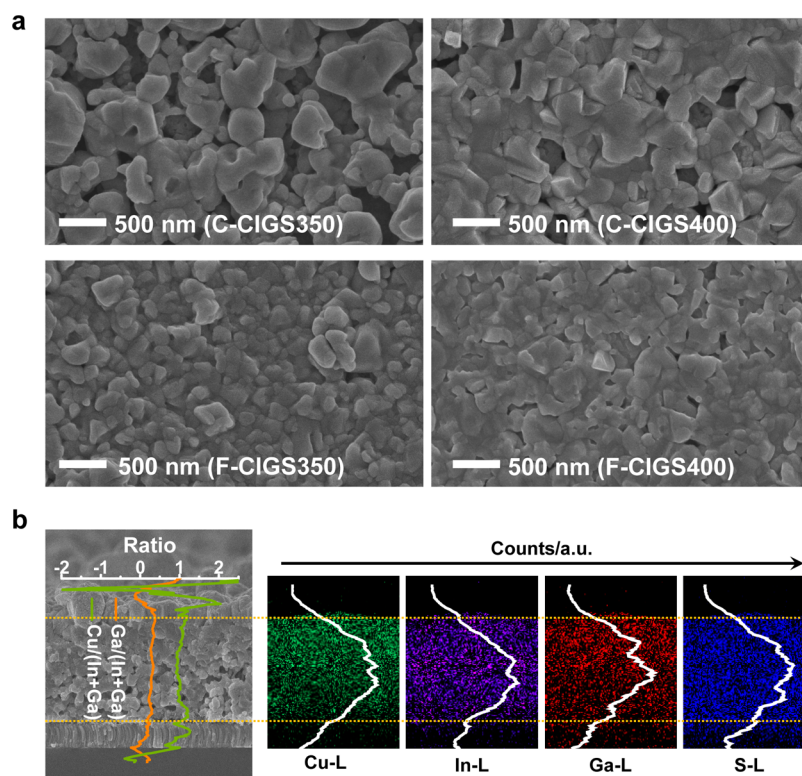
Figure 4. (a) Microstructure evolution of CIGS film as a function of sulfurization temperature ranging from 350 to 400 °C. The films were annealed in a N_2 + H_2S (5%) atmosphere in a tube furnace. (b) The linear depth profiles determined by EDX show the metallic distribution of the absorber layer. The graph superimposed on the SEM image indicated a uniform compositional distribution. The average ratio of Cu/(In+Ga) is ∼0.93 and Ga/(In+Ga) is ∼0.3.

Table 1. Composition Ratio at the Surfaces of the CIGS Films Using a Formate-Containing Ink Annealed at 400 °C, As Determined by EDX

composition ratio (as-prepared)		composition ratio (after sulfurization)		
Cu/(In + Ga)	In/(In + Ga)	Cu/(In + Ga)	In/(In + Ga)	S/Cu
0.98	0.72	0.97	0.73	2.42

layer. The relative compositional depth profile of metallic components for the F-CIGS400 absorber layer indicated a relatively uniform compositional distribution (Figure 4b). Aqueous ink-based thin-film solar cells were constructed following the conventional configuration of Mo-coated glass/ $Cu(In,Ga)S_2/CdS/i$-ZnO/ITO/Ni/Al without an antireflection layer. According to current density−voltage ($J−V$) characteristics, the F-CIGS400-based device showed the highest efficiency (η) of 7.04%, with an open-circuit voltage (V_{oc}) of 540 mV, a short circuit current density (J_{sc}) of 27.4 mA cm^{-2}, and fill factor (FF) of 47.7% (Figure 5a). In contrast, the device employing C-CIGS400 exhibited a much lower efficiency of 1.24%. The performance parameters are listed in Table 2. The distinctively low efficiency for the C-CIGS400 device resulted from the relatively porous, rough microstructure, and the undesirable formation of secondary phases such as the Cu−Au ordered phase and ternary sulfide, both of which are believed to deteriorate the J_{sc} and FF. Remaining chlorine impurities might also cause the spontaneous formation of copper vacancies;[21] these vacancies tend to increase the free carrier concentration, reducing the width of the space charge region and in turn degrading the collection efficiency of generated charge carriers. Interestingly, poor performance parameters were obtained for

the $Cu(In,Ga)S_2$ solar cell employing the absorber layer, N-CIGS400, prepared from all nitrate-based ink (Figure S4 in Supporting Information). Note that the nucleophilic strength difference between nitrate and formate anions is negligible. This implies that the hydrolysis tendency affected by the chemical nature (i.e., basicity) of the anion plays a dominant role in determining the chemical/crystalline structure for the aqueous ink-derived CIGS absorber layer. All nitrate-based ink prefers predominantly hydroxo ligands instead of oxo ligands, leading to insufficient formation of M−O−M framework.

Figure 5b shows the external quantum efficiency (EQE) for F-CIGS400 and C-CIGS400 solar cells. For the F-CIGS400 device, a broad middle band response and a sharp tail toward the band gap cutoff indicated suitable carrier collection. The quantum efficiency loss at a short wavelength range below ∼500 nm can be ascribed to absorption in the buffer layer because our buffer layer thickness was ∼60 nm, which is slightly thicker than those reported by others.[22,23] The device derived from sample F-CIGS400 showed a maximum quantum efficiency of 84% at 550 nm, and the band gap was determined to be 1.48 eV by fitting a plot of $[E \ln(1 − EQE)]^2$ vs E near the band edge. The C-CIGS400 device showed a maximum quantum efficiency of 36% at 540 nm, with a band gap of 1.51 eV. This value is relatively low as compared to typical band gap energy for $Cu(In,Ga)S_2$ (∼1.7 eV). It is speculated that the discrepancy of band gap is caused by insufficient crystallization because of low annealing temperature. Although our aqueous ink derived precursor film contains homogeneous distribution of Cu−In−Ga, the sulfurization at 400 °C might not provide sufficient thermal energy to fully crystallize into chalcopyrite structure. The trace of ternary sulfide phase as $CuIII_5S_8$ would
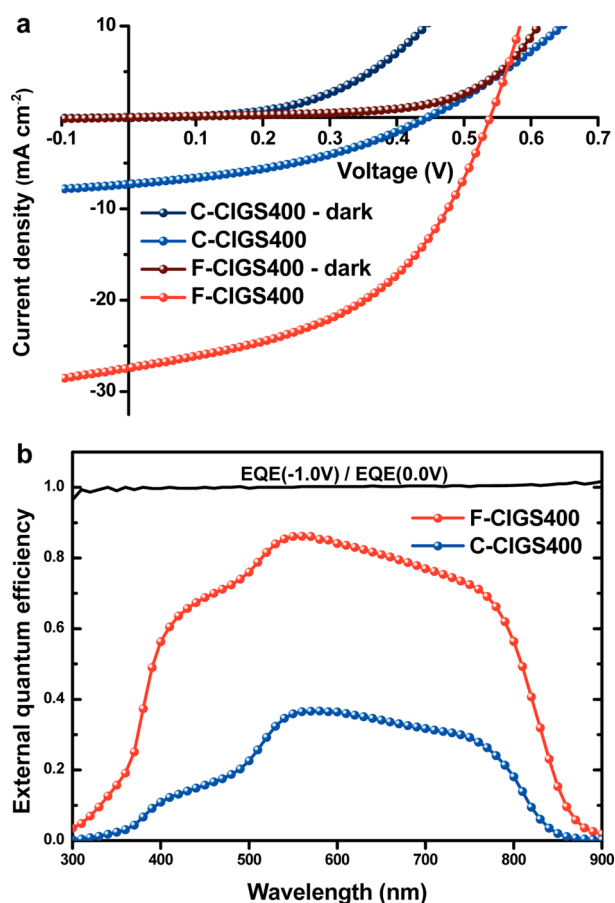
Figure 5. (a) Current density–voltage (J–V) characteristics of the CIGS solar cell annealed at 400 °C for both precursor usages. (b) External quantum efficiency (EQE) curve of the C-CIGS400 and F-CIGS300 cells. F-CIGS400 has 26.1 mA cm^{-2} current density calculated from EQE, also C-CIGS has 6.67 mA cm^{-2}. A bias ratio EQE(−1.0 V)/EQE(0.0 V) (black curve) for the F-CIGS400 device is also shown.

lower the band gap of our CIGS film.[24] Therefore, the resulting absorber layer has relatively uniform composition as shown in Figure 4b, whereas the band gap is relatively lower than the typical band gap of CIGS.

The ratio of EQE at −1 and 0 V, that is, [EQE(−1.0 V)/ EQE(0.0 V)], is indicative of the degree of carrier collection efficiency. The equivalent value (i.e., a ratio of 1) in a full wavelength implies the ideal charge collection. Good absorber quality of F-CIGS400 was evidently observed in the EQE bias-ratio plot (black line in Figure 5b). The slightly increasing trend in the ratio at a longer wavelength might be attributable to the poor minority-carrier collection from our absorber layer with a large band gap energy (∼1.5 eV).[22] As a comparison, the efficiency was measured to be 4.1% for the F-CIGS350 solar cell (Figure S5 in Supporting Information). The quantum

efficiency of the F-CIGS350 cell is shown in Figure S6 (Supporting Information), and the device parameters are listed in Table S1 (Supporting Information).

Successful demonstration of the Cu(In,Ga)S$_2$ solar cell at 400 °C, compatible with plastic substrates, suggests the possibility of realizing flexible, solution−processed photovoltaic devices. We fabricated aqueous ink-based Cu(In,Ga)S$_2$ solar cells on PI substrate, following identical procedures as used above. Figure 6a shows a photograph of the device fabricated on the PI substrate. To test the flexibility of the F-CIGS400 device on the PI substrate, a bending test was performed. The initial J−V characteristics of the flexible solar cell showed an efficiency of 5.6%, with a V_{oc} of 489 mV, J_{sc} of 25.32 mA cm^{-2}, and FF of 44.8% (Figure 6b). The discrepancy of the flexible device with respect to the rigid counterpart likely arose from the roughness of the initial Mo-coated PI substrate. Figure S7 (Supporting Information) shows the surface images of Mo-coated substrates. The glass-based substrate was much smoother than the PI based-one. Furthermore, as shown in Figure S8 (Supporting Information), an unevenly overgrown microstructural morphology was observed for the F-CIGS400 absorber layer on the PI substrate. The device was repeatedly bent between two parallel plates with a radius of 7 mm at room temperature in air (right side of Figure 6a), and the cell performance was determined after every 25 bending cycles (Figure 6c). The variation of electrical device parameters (P) obtained during repetitive bending is represented by $P_{(n)}/P_{(o)}$, where $P_{(o)}$ is the initial parameter value, and $P_{(n)}$ is the parameter value measured when flattened after a certain number of bending cycles. It should be noted that our solution-deposited flexible device remained intact with a reasonable mechanical tolerance against bending stress.[25] Compared to the initial state, both FF and J_{sc} maintained nearly unchanged after up to 300 cycles, and a slight reduction in both V_{oc} and η were observed after 100 repeated bending cycles. Slight increase in J_{sc} during the repeated bending test was caused by light soaking effect during bending test. It is speculated that the degradation of V_{oc} is ascribed to the strengthened electron scattering by strain-induced defects/ cracks formed in the absorber and Mo back-electrode layer.

Although the efficiency of our cell is lower than those (7.7– 8.3%) of other cells produced by alcohol solvent-based methods,[4,5] the improvement in device performances would be expected in further studies after resolving several processing issues. One of plausible reasons for relatively low efficiencies is attributable to a bilayered absorber microstructure, as shown in cross-sectional SEM (Supporting Information Figure S3). The charge carrier trapping at the junction between the fine- and coarse-grained layers and less dense morphology of lower layer can contribute to an increase in the series resistance, leading to the loss in efficiency to some extent. It can be suggested that with further optimized sulfurization process, the homogeneous, junction-free CIGS absorber layer would be achievable. In

Table 2. Device Performance of CIGS Solar Cells Fabricated Using Two Different Precursor Inks

sample name	J_{sc} (mA cm^{-2})	V_{oc} (V)	FF (%)	η (%)	$R_s{}^a$ (Ω·cm^2)	$R_{sh}{}^b$ (Ω·cm^2)
C-CIGS400	7.32	0.44	38.1	1.24	14.65	1807.1
F-CIGS400	27.40	0.54	47.7	7.04	1.09	1040.6

^{a}Series resistance (R_s) is determined based on voltage difference at the maximum power points between the one-sun J–V curve and the dark J–V curve, which is shifted by the short circuit current density J_{sc}, as proposed by Aberle.[26] ^{b}Shunt resistance (R_{sh}) is the change in the voltage for change in the current density at 0 V on the dark J_{sc}–V_{oc} curve.[26]
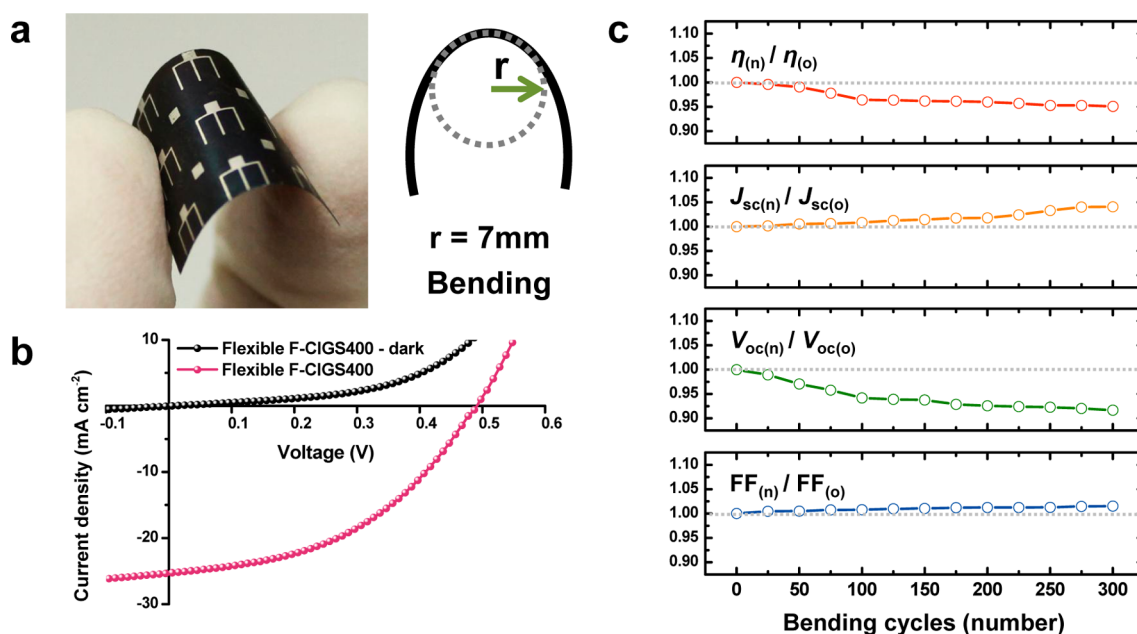
Figure 6. (a) Photograph of flexible F-CIGS400 solar cells on PI substrates, and schematics showing the mechanical bend test conditions (right). (b) Current density–voltage ($J-V$) characteristics of the flexible CIGS solar cell annealed at 400 °C. (c) The variations in the electrical parameters during the repeated bending cycles under a fixed strain. The cell parameters were measured when the substrate was flattened after a certain number of bending cycles.

addition, the incorporation of MgF_2 antireflection layer is currently underway to improve the cell efficiency. We believe that resolving these issues allows us to produce large area, low cost flexible CIGS solar cells with much higher efficiencies, highly desirable for photovoltaic applications

3. CONCLUSIONS

In summary, our simple aqueous-based deposition approach facilitated a low temperature process, allowing for CIGS photovoltaic devices on a plastic substrate. The aqueous ink, which was readily achievable without the involvement of a complex particle synthesis step and the usage of highly toxic solvents and organic additives, enabled a convenient method for single-phase, compositionally uniform, large-grained CIGS absorber layers. Through a combined spectroscopic analysis using Raman spectroscopy and XPS, it was revealed that the introduction of formate anions lead to a preferred M-O-M framework and phase transformation capability into the CIGS phase. The resulting CIGS thin-film solar cell showed a conversion efficiency of 7.04% on a rigid substrate (Mo-coated soda lime glass) and 5.60% on a flexible PI substrate, with thermal processability at temperatures as low as 400 °C. The device fabricated on a PI substrate operated reliably even after 300 cycles of a bending test. It is believed that our simple, green chemistry-based approach represents the first step toward realizing low-cost, scalable, highly efficient CIGS absorber layers for flexible solar cells.

4. EXPERIMENTAL METHOD

CIGS Film Preparation and Device Fabrication. Precursor solutions were prepared by dissolving the appropriate amounts of $Cu(HCOO)_2 \cdot 4H_2O$ (98%, Alfa Aesar), $In(NO_3)_3 \cdot xH_2O$ (99.9%, Sigma-Aldrich), and $Ga(NO_3)_3 \cdot xH_2O$ (99.9%, Sigma-Aldrich) in deionized water. The molar ratio of Cu/In/Ga was 0.98:0.72:0.28, and the total concentration of precursor was ~1.0 M. Other precursor solutions incorporating either $CuCl_2$ (99.9%, Sigma-Aldrich) or $Cu(NO_3)_2 \cdot 3H_2O$ (99%, Sigma-Aldrich) was also prepared using the

same In and Ga nitrates. To provide the sodium ion in the absorber layer, sodium formate ($NaHCO_2$, Sigma-Aldrich) was dissolved in the formate-containing ink, whereas sodium chloride (NaCl, Sigma-Aldrich) was used in the chlorine-containing inks and sodium nitrate ($NaNO_3$, Sigma-Aldrich) was used in the all nitrate based ink. The precursor solution was spin-coated on either Mo-coated soda lime glass or PI (UPILEX-S, Ube Industries Ltd.) substrate. A Mo layer of ~500 nm thickness was deposited by DC sputtering. The absorber layers were spin-coated, followed by preannealing on a hot plate at 350 °C for 10 min in an ambient atmosphere. A single coating of the precursor solution led to formation of a film with a thickness of ~80 nm; multiple coatings were performed to achieve a desirable thickness. We followed the annealing procedure introduced by Kapur et al.[27] after a slight modification from H_2Se to H_2S gas. The prepared films were then annealed in a tube furnace at a temperature of either 350 or 400 °C. The sulfurization process was consisted of a heating up to target temperature under 5% H_2/Ar gas, followed by a hold for 30 min under 5% H_2S/N_2 atmosphere to convert the precursor films into the CIGS absorber. The sulfurized absorber films were processed into photovoltaic devices using methods including chemical bath deposition of CdS (~60 nm), RF sputtering of i-ZnO (~50 nm), RF sputtering of ITO (~200 nm), and thermal evaporation of a patterned Ni/Al grid as the top electrode. The final devices (2 cm × 3 cm) were mechanically scribed into cells with an area of 0.15 cm². We measured the current–voltage ($I-V$) characteristics of our aqueous precursor-derived CIGS solar cells measured in the dark and under AM 1.5 illumination. The integrated intensity was reduced to 1000 W m^{-2} using neutral density filters. The bending test was comprised of more than 300 cycles of rolling and unrolling on a cylinder with a 7 mm radius of curvature, as shown in Figure 6a.

Characterization. Thermal analysis of the aqueous precursor inks was performed using thermogravimetric differential scanning calorimetry (SDT Q600, TA Instruments). Structural and compositional analyses were performed using a field emission scanning electron microscope equipped with energy-dispersive X-ray spectroscopy (FESEM, JSM-6701F, JEOL). The phase/chemical characterizations of films were performed using an X-ray diffraction (XRD, D/Max-2500H, Rigaku) with Cu Kα radiation (λ = 0.15406 nm), a Raman spectroscopy (Lab Ram ARAMIS, Horiba Jobin-Yvon), and an X-ray photoelectron spectroscopy (XPS-depth profile, monochromated Kα,

17746

dx.doi.org/10.1021/am504194t | ACS Appl. Mater. Interfaces 2014, 6, 17740–17747

Thermo). Prior to XPS analysis, the sputtering in area of 2×2 mm^2 was performed with an Ar$^+$ ion gun (0.2 kV) to clean the surfaces of the samples. All binding energies were readjusted with respect to carbon.

ASSOCIATED CONTENT

Supporting Information

Detailed description of the experimental methods, TG analysis of three different precursor derived ink, In 3d5/2 and Ga 2p3/2 XPS of the CIGS films during annealing process, XRD patterns for the F-CIGS and C-CIGS films, cross sectional SEM image of F-CIGS400 solar cell, EDX depth profile showing the compositional distribution of F-CIGS400, performance comparison of CIGS thin film solar cells, AFM showing comparison of Mo morphology on SLG and PI, and SEM image of the surface of the F-CIGS400 fabricated on a PI substrate. This material is available free of charge via the Internet at http://pubs.acs.org.

AUTHOR INFORMATION

Corresponding Author
*Tel.: +82 2 2123 2855. Fax: +82 2 312 5375. Email: jmoon@yonsei.ac.kr.

Notes
The authors declare no competing financial interest.

ACKNOWLEDGMENTS

REFERENCES

(1) Hibberd, C. J.; Chassaing, E.; Liu, W.; Mitzi, D. B.; Lincot, D.; Tiwari, A. N. Non-Vacuum Methods for Formation of Cu(In, Ga)(Se, S)$_2$ Thin Film Photovoltaic Absorbers. *Prog. Photovoltaics* **2010**, *18*, 434−452.

(2) Habas, S. E.; Platt, H. A. S.; Hest, M. F. A. M.; Ginley, D. S. Low-Cost Inorganic Solar Cells: From Ink to Printed Device. *Chem. Rev.* **2010**, *110*, 6571−6594.

(3) Todorov, T. K.; Gunawan, O.; Gokmen, T.; Mitzi, D. B. Solution-Processed Cu(In,Ga)(S,Se)$_2$ Absorber Yielding a 15.2% Efficient Solar Cell. *Prog. Photovoltaics* **2013**, *21*, 82−87.

(4) Park, S. J.; Cho, J. W.; Lee, J. K.; Shin, K.; Kim, J. H.; Min, B. K. Solution Processed High Band-Gap CuInGaS$_2$ Thin Film for Solar Cell Applications. *Prog. Photovoltaics* **2014**, *22*, 122−128.

(5) Uhl, A. R.; Fella, C.; Chirilă, A.; Kaelin, M. R.; Karvonen, L.; Weidenkaff, A.; Borca, C. N.; Grolimund, D.; Romanyuk, Y. E.; Tiwari, A. N. Non-Vacuum Deposition of Cu(In,Ga)Se$_2$ Absorber Layers from Binder Free, Alcohol Solutions. *Prog. Photovoltaics* **2012**, *20*, 526−533.

(6) Chirilă, A.; Buecheler, S.; Pianezzi, F.; Bloesch, P.; Gretener, C.; Uhl, A. R.; Fella, C.; Kranz, L.; Perrenoud, J.; Seyrling, S. Highly Efficient Cu(In,Ga)Se$_2$ Solar Cells Grown on Flexible Polymer Films. *Nat. Mater.* **2011**, *10*, 857−861.

(7) Kessler, F.; Herrmann, D.; Powalla, M. Approaches to Flexible CIGS Thin-Film Solar Cells. *Thin Solid Films* **2005**, *480*, 491−498.

(8) Kessler, F.; Rudmann, D. Technological Aspects of Flexible CIGS Solar Cells and Modules. *Sol. Energy* **2004**, *77*, 685−695.

(9) Seo, J.; Jeon, J.; Hwang, Y.; Park, H.; Ryu, M.; Park, S.; Bae, B. Solution-Processed Flexible Fluorine-Doped Indium Zinc Oxide Thin-Film Transistors Fabricated on Plastic Film at Low Temperature. *Sci. Rep.* **2013**, *3*, 2085.

(10) Briggs, D.; Seah, M. P. *Practical Surface Analysis: By Auger and X-ray Photoelectron Spectroscopy*; Wiley: New York, 1983.

(11) Moulder, J. F.; Chastain, J.; King, R. C. *Handbook of X-ray Photoelectron Spectroscopy: A Reference Book of Standard Spectra for Identification and Interpretation of XPS Data*; Physical Electronics Eden Prairie: Chanhassen, MN, 1995.

(12) Barr, T. L. Recent Advances in X-ray Photoelectron Spectroscopy Studies of Oxides. *J. Vac. Sci. Technol. A* **1991**, *9*, 1793−1805.

(13) Cushing, B. L.; Kolesnichenko, V. L.; O'Connor, C. J. Recent Advances in the Liquid-Phase Syntheses of Inorganic Nanoparticles. *Chem. Rev.* **2004**, *104*, 3893−3946.

(14) Brinker, C. J.; Scherer, G. W. *Sol−Gel Science: The Physics and Chemistry of Sol−Gel Processing*; Elsevier: London, U.K., 1990.

(15) Hench, L. L.; West, J. K. The Sol−Gel Process. *Chem. Rev.* **1990**, *90*, 33−72.

(16) Chase, M. W.; Curnutt, J.; Prophet, H.; McDonald, R.; Syverud, A. N. JANAF Thermochemical Tables, 1975 Supplement. *J. Phys. Chem. Ref. Data* **1975**, *4*, 1−176.

(17) Theodoropoulou, S.; Papadimitriou, D.; Rega, N.; Siebentritt, S.; Lux-Steiner, M. C. Raman and Photoreflectance Study of CuIn$_{1−x}$Ga$_x$Se$_2$ Epitaxial Layers. *Thin Solid Films* **2006**, *511*, 690−694.

(18) Klugius, I.; Miller, R.; Quintilla, A.; Friedlmeier, T. M.; Blázquez-Sánchez, D.; Ahlswede, E.; Powalla, M. Growth Mechanism of Thermally Processed Cu(In,Ga)S$_2$ Precursors for Printed Cu-(In,Ga)(S,Se)$_2$ Solar Cells. *Phys. Status Solidi RRL* **2012**, *6*, 297−299.

(19) Neisser, A.; Hengel, I.; Klenk, R.; Mattes, T. W.; Alvarez-Garcia, J.; Perez-Rodriguez, A.; Romano-Rodriguez, A.; Lux-Steiner, M. C. Effect of Ga Incorporation in Sequentially Prepared CuInS$_2$ Thin Film Absorbers. *Sol. Energy Mater. Sol. Cells* **2001**, *67*, 97−104.

(20) Camus, C. *Doktor der Naturwissenschaften*; Freie Universität, Berlin, 2008.

(21) Guo, Q.; Ford, G. M.; Yang, W. C.; Walker, B. C.; Stach, E. A.; Hillhouse, H. W.; Agrawal, R. Fabrication of 7.2% Efficient CZTSSe Solar Cells Using CZTS Nanocrystals. *J. Am. Chem. Soc.* **2010**, *132*, 17384−17386.

(22) Chopra, K. L.; Paulson, P. D.; Dutta, V. Thin-Film Solar Cells: An Overview. *Prog. Photovoltaics* **2004**, *12*, 69−92.

(23) Shafarman, W. N.; Klenk, R.; McCandless, B. E. Device and Material Characterization of Cu(InGa)Se$_2$ Solar Cells with Increasing Band Gap. *J. Appl. Phys.* **1996**, *79*, 7324−7328.

(24) Qasrawi, A. F.; Gasanly, N. M. Photoelectronic and Electrical Properties of CuIn$_5$S$_8$ Single Crystals. *Cryst. Res. Technol.* **2003**, *38*, 1063−1070.

(25) Kim, A.; Won, Y.; Woo, K.; Kim, H.; Moon, J. Highly Transparent Low Resistance ZnO/Ag Nanowire/ZnO Composite Electrode for Thin Film Solar Cells. *ACS Nano* **2013**, *7*, 1081−1091.

(26) Pysch, D.; Mette, A.; Glunz, S. A Review and Comparison of Different Methods to Determine the Series Resistance of Solar Cells. *Sol. Energy Mater. Sol. Cells* **2007**, *91*, 1698−1706.

(27) Kapur, V. K.; Bansal, A.; Le, P.; Asensio, O. I. Non-Vacuum Processing of CuIn$_{1−x}$Ga$_x$Se$_2$ Solar Cells on Rrigid and Flexible Substrates using Nanoparticle Precursor Inks. *Thin Solid Films* **2003**, *431*, 53−57.